Open access • Journal Article • DOI:10.1016/J.MSEA.2015.10.094

Superplasticity of a nano-grained Mg–Gd–Y–Zr alloy processed by high-pressure torsion — Source link

Reza Alizadeh, Reza Alizadeh, Reza Mahmudi, Ahw Ngan ...+2 more authors

Institutions: University of Tehran, University of Hong Kong, University of Southampton

Published on: 10 Jan 2016 - Materials Science and Engineering A-structural Materials Properties Microstructure and Processing (Elsevier)

Topics: Superplasticity, Grain Boundary Sliding, Severe plastic deformation, Friction stir processing and Strain rate

Published in *Materials Science and Engineering A*, 651, 2016, pp786-794. doi: 10.1016/j.msea.2015.10.094

Superplasticity of a nano-grained Mg–Gd–Y–Zr alloy processed by high-pressure torsion

R. Alizadeh[a,b], R. Mahmudi[a,*], A.H.W. Ngan[b], Y. Huang[c], T.G. Langdon[c]

[a]*School of Metallurgical and Materials Engineering, College of Engineering, University of Tehran, Tehran, Iran.*
[b]*Mechanical Engineering Department, The University of Hong Kong, Pokfulam Road, Hong Kong.*
[c]*Materials Research Group, Faculty of Engineering and the Environment, University of Southampton, Southampton SO17 1BJ, U.K.*

Abstract

While most of the reports on Mg-Gd-Y-Zr alloys report superplasticity after extrusion or friction stir processing, it is important to investigate superplasticity in these alloys after other severe plastic deformation processes having greater grain refinement capability. Accordingly, superplasticity was studied in an Mg–9Gd–4Y–0.4Zr (GW94) alloy after different high-pressure torsion (HPT) conditions. The HPT was performed at room temperature under an applied pressure of 6.0 GPa for up to 16 turns. TEM microstructural characterization revealed that the grain size was reduced from an initial value of ~8.6 μm in the extruded condition to ~95 ± 10 and ~85 ± 10 nm after 8 and 16 turns, respectively. A shear punch testing method was used for evaluation of superplasticity at 573, 623, 673 and 723 K. Maximum strain rate sensitivities of ~0.51 ± 0.05 and ~0.48 ± 0.05 were obtained at 623 K for the material processed through 16 and 8 turns, respectively. This strain rate sensitivity and an activation energy of ~100 ± 5 kJ mol^{-1} suggests the occurrence of grain boundary sliding in the superplastic region.

***Keywords**:* High-pressure torsion; Mg–Gd–Y–Zr alloys; Nano-grained metals; Shear punch testing; Superplasticity

*Corresponding author: e-mail: mahmudi@ut.ac.ir, Phone: +98 21 8208 4137, Fax: +98 21 8800 6076

1. Introduction

Magnesium alloys, as the lightest structural materials, have been the subject of much research in recent years because of their numerous advantages such as low density and high specific strength. Despite these advantages, Mg alloys suffer from poor room temperature formability because of the limited slip systems in their hexagonal close-packed (hcp) structure [1]. In order to overcome these limitations, attempts have been made to enhance their formability through the use of superplastic deformation which will permit the fabrication of light structural components having complex shapes [2–4]. Excellent thermal stability was reported recently in a series of Mg–Gd alloys and this permitted the occurrence of extensive superplasticity in these alloys [5]. Nevertheless, most of the investigations of the Mg–Gd alloys reported superplasticity after simple extrusion [5,6] or friction stir processing (FSP) [7–9] and the minimum grain sizes attained by these methods were of the order of ~3 μm [8]. This suggests that it may be advantageous to evaluate the occurrence of superplasticity in these alloys after processing using severe plastic deformation (SPD) processes where there is a capability of achieving an even greater level of grain refinement.

It is now well established that processing by high-pressure torsion (HPT) provides the capability of producing materials with extremely fine grain sizes which are suitable for achieving superplastic flow [10]. There are now several reports of superplastic flow in metals processed using SPD techniques [11,12] and Table 1 provides a comprehensive summary of the investigations reported to date for superplastic flow in metals processed by HPT [13–19]: in this table, the HPT processing conditions are listed in columns 2–4, the resultant grain sizes are listed in column 5 and the superplastic testing conditions are

given in columns 6–8 where data are included only when the maximum elongations exceed the critical requirement of a tensile elongation of at least 400% for superplastic flow [20]. It is readily apparent from inspection of Table 1 that all of these materials exhibit excellent superplastic properties with a maximum elongation of 1330% reported for an Mg–8Li alloy [19]. Nevertheless, there is only a single report of superplasticity in an Mg–10Gd alloy [17] and thus it is important to fully investigate superplasticity of the HPT-processed Mg-Gd alloys.

Although tensile testing is the conventional standard procedure for delineating superplastic flow, other testing methods are now available for measuring the strain rate sensitivity (SRS) and thus providing an indirect method for identifying the possible occurrence of superplasticity. For example, shear punch testing (SPT) was recently introduced as a suitable technique for measuring SRS in different materials processed by SPD and a summary of the results available to date is given in Table 2 [6,21–24]. It is important to note also that the SPT-tensile correlation was already validated several years ago [25]. The advantages of studying superplasticity by SPT was reviewed earlier [21] and it includes the requirement for using only very small amounts of material as is readily produced using HPT processing. Thus, the objective of this research was to use SPT to examine the possible occurrence of superplasticity in an Mg–Gd–Y–Zr alloy after processing through different HPT conditions. It should be noted also that SPT has the advantage of being conducted locally and thus on selected positions of the radius of HPT discs.

2. Experimental material and procedures

An Mg–9 wt% Gd–4 wt%Y–0.4 wt% Zr (GW94) alloy was prepared from high purity Mg and Mg–30Gd, Mg–30Y and Mg–30Zr master alloys which were melted in an electric furnace under a covering flux. The molten material was poured into a steel die preheated to 573 K using a tilt-casting system to minimize casting defects and any melt turbulence. Extrusion was conducted to a diameter of 10 mm using an extrusion ratio of 19:1 at a temperature of 673 K and a graphite lubricant.

Thin slices with thicknesses of ~1.2 mm were cut perpendicular to the extrusion direction using an electro-discharge machine (EDM) and both sides of these disks were carefully polished using abrasive papers to prepare a series of samples with thicknesses of ~0.80 mm. The HPT processing was performed under quasi-constrained conditions [26]. The anvils on a quasi-constrained HPT facility contain shallow round cavities having depths which are a little less than the one-half thickness of the HPT sample. These cavities prevent significant lateral flow of the sample and the reduced depth ensures there is no direct contact between the anvils during the HPT operation. All processing was conducted at room temperature under an applied pressure, P, of 6.0 GPa. Torsional straining was applied by rotating the lower anvil at a constant speed of 1 rpm through total numbers, N, of 1/2, 1, 2, 4, 8 and 16 revolutions. No damage or cracking was observed after processing by HPT through different numbers of revolutions. The final thicknesses of the HPT discs were in the range of ~0.500-0.580 mm.

An Hitachi S-3400N variable pressure scanning electron microscope (SEM) and an FEI Tecnai G2 20 S-TWIN scanning transmission electron microscope (TEM) with a

maximum operating voltage of 200 kV were used to study the microstructures of the samples after different HPT conditions. The samples for the SEM investigations were etched with an acetic-picral solution. TEM samples were cut by punching at a radius of 1.5 mm from the center of the HPT discs and were prepared by ion beam milling (IBM). After grinding the HPT samples to ~100 μm thickness, their thicknesses were further reduced to ~20 μm with a dimpler machine and the TEM samples were finally prepared by IBM using a milling angle of 12° with a voltage of 4 kV.

The occurrence of superplasticity was evaluated after HPT processing using SPT, where full details were given earlier [27]. The SPT was performed at temperatures of 573, 623, 673 and 723 K under strain rates in the range from 3.3×10^{-3} to 2.7×10^{-1} s^{-1} using a screw-driven MTS testing system equipped with a three-zone split furnace. A shear punch fixture with a 2.957 mm diameter flat cylindrical punch and 3.044 mm diameter receiving hole was used for SPT. The dimensions of the HPT discs were suitable for the SPT die and it was possible to perform SPT directly without any sizing or cutting. Both sides of the HPT discs were ground by SiC abrasive paper (grade 800) to remove the roughness on the surfaces of the HPT samples. HPT samples were put on the center of the SPT die which means the shear deformation is performed at a radius of ~1.5 mm from the center of the HPT discs. The load, F, was measured automatically as a function of the punch displacement and the data were recorded by appropriate software to determine the shear stress, τ, on the tested material using the relationship [28]

$$\tau = \frac{F}{\pi D t} \qquad (1)$$

where t is the specimen thickness and D is the average of the punch and die hole diameters. The SPT curves were then plotted as shear stress against normalized punch displacement.

3. Experimental results

3.1 Microstructural evolution during HPT processing

When a thin disk is processed by HPT under an applied pressure, the equivalent von Mises strain, ε, imposed on the disk by torsional straining is given by the relationship [29]

$$\varepsilon = \frac{2\pi N r}{h\sqrt{3}} \tag{2}$$

where r is the radial distance from the center of the disk and h is the initial thickness of the sample. Eq.(2) shows that the strain varies across the disk. Variations of strain, microstructure and hardness both across and within the HPT discs are summarized elsewhere [10]. Since the shear punch tests were conducted at a radial distance of $r = 1.5$ mm from the centers of the samples, the equivalent strains were calculated for these radial positions and they are recorded in Table 3. For consistency between all results, all of the microstructural characterizations were also performed at this radial distance. It is readily evident from Table 3 that these positions represent a very large span of strains from ~4 to ~145 and this will affect the microstructure and hence the superplastic behavior.

In the initial extruded condition prior to HPT, the material displayed a fairly equiaxed and uniform grain structure with an average grain size of ~8.6 μm: a detailed microstructural characterization of the extruded condition was given earlier [30]. SEM micrographs of the alloy at r = 1.5 mm are shown in Fig. 1 after (a) 1/2, (b) 2, (c) 8 and (d) 16 HPT turns. During HPT, the imposition of an applied pressure of 6.0 GPa together with the torsional straining at room temperature leads to extensive grain refinement. As is apparent from Fig. 1, the most important feature of the microstructures after 1/2 turn and 2 turns is the presence of severely twinned grains. Because of the exceptional grain refinement occurring after 8 and 10 turns, the microstructures of these samples were examined by TEM and the related images are shown in Fig. 2 after (a) 8 and (b) 16 turns. Very small grains were visible in both of these microstructures and measurements gave average grain sizes of ~95 ± 10 and ~85 ± 10 nm after 8 and 16 HPT turns, respectively. It was also apparent that the microstructures generally become more uniform with increasing numbers of turns and the grain boundaries become better defined.

SEM and TEM micrographs revealed that some cuboidal precipitates, in the range of 50 nm to 2 μm, exist in the microstructure of the alloy which may have some interactions with grain boundaries during high temperature plastic deformation. To evaluate the size and distribution of the Gd- and Y-rich precipitates, TEM micrographs and the corresponding elemental maps are shown in Figs. 3 and 4 after 8 and 16 turns, respectively. It is apparent from Fig. 4 that the Gd- and Y- rich precipitates are smaller and more uniformly distributed after 16 turns, thereby demonstrating that increasing numbers of turns leads to a refinement in both the grain size and the precipitate size. It should be noted that larger particles, in the range 1-2 μm, were distributed non-uniformly

in the microstructure and their volume fraction was smaller than the nanometer precipitates observed in Figs. 3 and 4. To analyze the crystal structure and chemical composition of the precipitates more precisely, a selected area electron diffraction (SAED) pattern and energy-dispersive X-ray spectroscopy (EDS) from a cuboidal precipitate are presented in Fig. 5. The SAED pattern shows that this precipitate has a face-centered cubic (FCC) crystal structure with a ≈ 0.54 ± 0.2 nm. The EDS results also indicate that the chemical composition of this precipitate is close to $Mg(Gd,Y)_4$. However, the results of EDS analyses on approximately 10 similar precipitates demonstrated that the chemical composition of these cuboidal precipitates lie in the range of $Mg(Gd,Y)_2$ to $Mg(Gd,Y)_5$. Also, it should be mentioned that, in accordance with an earlier study [30], the EDS results confirm the presence of some small Zr-rich precipitates in the microstructure of the alloy.

3.2 Superplastic behavior after HPT processing

It is reasonable to anticipate that the different microstructures attained after these deformation processes will affect the superplastic behavior of the material. To investigate this effect, Fig. 6a shows representative plots of shear stress against the normalized displacement for samples processed through 8 turns and then tested at 623 K in SPT using a range of shear strain rates from 6.7×10^{-3} to 1.3×10^{-1} s^{-1}. The ultimate shear strength (USS, τ_m) can be obtained from these curves and then used to calculate the strain rate sensitivity.

As noted earlier, the high-temperature shear flow stress, τ, is related to the shear strain rate, $\dot{\gamma}$, by a power–law relationship [6]

$$\left(\frac{\dot{\gamma}T}{G}\right) = \left(\frac{Ab}{k}\right)\left(\frac{b}{d}\right)^{p}\left(\frac{\tau}{G}\right)^{\frac{1}{m}} \exp\left(\frac{-Q}{RT}\right) \tag{3}$$

where A is a material parameter, b is the Burgers vector, k is Boltzmann's constant, d is the grain size, p is the inverse grain size exponent, G is the shear modulus, m denotes the strain rate sensitivity index, Q is the deformation activation energy, R is the universal gas constant and T is the absolute temperature.

From experimental data for the elastic constants of magnesium, the temperature dependence of the shear modulus is generally expressed as [31]

$$G\ (\text{MPa}) = 19200 - 8.6T\ (\text{K}) \tag{4}$$

Due to the constancy of Q at a given temperature, it is possible to determine the value of m from the relationship:

$$m = \left(\frac{\partial ln\left(\frac{\tau}{G}\right)}{\partial ln\left(\frac{\dot{\gamma}T}{G}\right)}\right)_{T} \tag{5}$$

Fig. 6b shows the variations of the normalized USS of the material after 8 turns plotted against the temperature-compensated shear strain rate for different testing temperatures. According to Eq. (5), the slopes of these curves give the corresponding values of m that are listed in Fig. 6b.

It is apparent that the dependency of USS on strain rate is linear at 573 K with $m \approx 0.33 \pm 0.05$. However, the dependency becomes sigmoidal with three distinct regions at

623 K and the region with maximum slope has $m \approx 0.48 \pm 0.05$ but at the higher temperatures of 673 and 723 K the slope is then reasonably linear. To obtain a better representation of data, the variation of m with test temperature is plotted in Fig. 6c. It is clear that the maximum strain rate sensitivity is achieved at 623 K where $m \approx 0.48 \pm 0.05$.

To investigate the severity of the grain growth at high temperatures, the microstructures of the material after SPT at 623 and 723 K are shown in Fig. 7. These microstructures were taken from the die area of the SPT samples. Grain size measurements showed that the grain size of the material increased from an initial value of ~95 ± 10 nm after 8 turns to ~14 ± 5 μm after SPT testing at 723 K. By contrast, the alloy exhibits reasonable thermal stability at 623 K where the grain growth is restricted.

After obtaining the optimum temperature of 623 K for achieving the highest SRS, shear punch tests were performed on samples processed for different numbers of HPT turns. The results are shown in Fig. 8 where SPT data of the extruded material is also included for comparison [6]. Figure 8a shows the variation of the USS with the temperature-compensated shear strain rate and Fig. 8b shows the variation of m with the numbers of turns in HPT. Thus, m increases from the initial value of ~0.13 ± 0.05 in the extruded condition to ~0.51 ± 0.05 after 16 turns. Also, the material shows a large value of $m \approx 0.48 \pm 0.05$ after 8 turns and therefore increasing the numbers of turns has only a minor effect after about 8 turns.

According to Eq. (3), the deformation activation energy may be calculated at constant shear strain rate as:

$$Q = \frac{R}{m}\left(\frac{\partial ln(\tau/G)}{\partial(1/T)}\right)_{\frac{\dot{\gamma}T}{G}} \quad (6)$$

Consequently, the normalized USS values are plotted against the reciprocal of temperature at constant temperature-compensated shear strain on a semi-logarithmic scale in Fig. 9 in order to calculate the activation energy of the material after 8 HPT turns. Calculations were made in the temperature range of 573–673 K in which the material showed a maximum value for the SRS and the average activation energy was determined as ~100 ± 5 kJ mol^{-1}.

4. Discussion

4.1. Grain and precipitate refinement during HPT processing

Microstructural characterization revealed that the microstructure of the material was severely twinned in the initial stages of deformation after 0.5 and 2 HPT turns. This matches an earlier report of the microstructure of a ZK60 magnesium alloy after HPT [15]. In low temperature deformation in hcp metals, deformation twinning occurs at the early stage of deformation and serves as an additional deformation mechanism to dislocation slip. Additionally, it has been reported that in magnesium alloys, above a critical value of the Zener-Holloman parameter (*Z*), twinning influences the dynamic recrystallization process and this produces a more effective grain refinement [32]. Accordingly, severely deformed microstructures at the initial stages of deformation by HPT can contribute in the grain refinement process with increasing numbers of turns.

The microstructures of the material after 8 and 16 HPT turns indicate that nano-size recrystallized grains are obtained after relatively large strains in the range of ~72–145 at room temperature. Previous studies on nickel and copper indicated that recrystallization

may occur below an homologous temperature of ~0.4 T_m when the accumulated strain during HPT rises above ~5, where T_m is the absolute melting temperature of the material [33]. Thus, although the situation may be different in Mg-Gd alloys, the results in this research confirm the occurrence of recrystallization during HPT processing at room temperature at large imposed strains.

It appears that the present average grain size of ~85 nm after 16 turns is the smallest grain size reported to date for the Mg–Gd alloy system. Nevertheless, similar exceptionally small grain sizes were reported earlier for other Mg alloys both after HPT and after using other deformation processes. For example, a grain size of ~85 nm was reported in an AZ31 alloy using two-step friction stir processing [34] and nanometer grains with an average size of ~30 ± 5 nm were generated in the surface layer of a single-phase AZ91D alloy using a surface mechanical attrition treatment [35]. Also, in experiments on the magnesium AZ61 alloy it was shown that HPT processing produced average grain sizes of ~220 and ~110 nm after HPT at 423 K and room temperature, respectively [13].

The present results indicate that not only the grains but also the Gd- and Y-rich precipitates are refined and become more uniformly distributed after larger strains (Figs. 3 and 4). Considering the relatively low diffusivity of the Gd and Y elements in Mg [36,37], it is concluded that severe deformation at room temperature both refines and redistributes these precipitates. It was reported earlier that these precipitates may restrict grain growth at high temperatures [30]. Therefore, it is anticipated that these fine morphologies of the precipitates in the samples processed for 8 and 16 turns will control the growth of these nanometer grains at high temperatures and this will be more effective

than the microstructure of the material before HPT processing where there were large precipitates having sizes of the order of several microns [30].

Regarding the crystal structure and chemical composition of the precipitates, the TEM results indicate that the cuboidal precipitates in the microstructure of the alloy have an FCC crystal structure ($a \approx 0.54 \pm 0.2$ nm) and their chemical compositions are in the range of $Mg(Gd,Y)_2$ to $Mg(Gd,Y)_5$. These results are consistent with previous studies which reported a similar FCC crystal structure with $a \approx 0.54–0.56$ nm and chemical compositions of $Mg_2(Gd,Y)$ and $Mg(Gd,Y)_5$ [38,39]. The EDS results also revealed that the Mg matrix contains about 2.07 and 1.07 at.% Gd and Y, respectively. According to the binary Mg-Gd which is not well established at low temperatures and the Mg-Y phase diagrams [40], Gd and Y have limited solubility in Mg at room temperature. Therefore, it appears that severe plastic deformation by HPT has led to the formation of a supersaturated solid solution (SSSS) in the Mg matrix.

4.2. The development of superplasticity at 623 K

The variation of the SRS after 8 turns shows that the *m*-value increases from an initial value of ~0.33 ± 0.05 at 573 K to ~0.48 ± 0.05 at 623 K and there is a further decrease at higher temperatures. The results show that, although the alley contains very small grain sizes in the range of ~100 nm, temperatures lower than 623 K are not suitable for superplastic deformation. The reason is that superplasticity is associated with the occurrence of grain boundary sliding (GBS) [41] and this requires the diffusion and redistribution of alloying elements during high temperature deformation. Accordingly, it

is reasonable to anticipate that, because of the low diffusion rates of Gd and Y in the Mg matrix, these lower deformation temperatures are not suitable for superplastic deformation in the Mg–Gd–Y alloys even when the grain sizes are within the nanometer range. The observed decrease in the *m*-values at higher temperatures above 623 K is due to an inherent grain growth of the nano-grained structure as demonstrated in Fig. 7 for a temperature of 723 K. By contrast, it was shown that the alloy exhibits reasonable thermal stability at 623 K where grain growth was restricted in the nano-grains.

With reference to the number of turns in HPT, the SPT results show that the *m*-value at 623 K increases from an initial value of ~0.16 ± 0.05 in the extruded condition [6] to ~0.48 ± 0.05 and 0.51 ± 0.05 after 8 and 16 turns, respectively. This increase in SRS is related to the finer microstructure of the material, with grains in the range of <100 nm after processing by HPT. In practice, however, the results suggest that 8 turns at room temperature represents an optimum processing procedure for achieving superplasticity in the GW94 alloy.

To investigate the deformation mechanism of the material in the superplastic region, it is necessary to consider both the activation energy and the strain rate sensitivity. The *m*–value of ~0.50 is associated with grain boundary sliding [41] and the activation energy of ~100 ± 5 kJ mol^{-1} is similar to the activation energy of ~92 kJ mol^{-1} for grain boundary diffusion in magnesium [42]. It is concluded, therefore, that GBS accommodated by grain boundary diffusion is the dominant deformation mechanism of the GW94 alloy in the superplastic region. This conclusion is consistent with the exceptionally fine-grained microstructure and the sigmoidal dependence of the SRS on the shear strain rate. It is also consistent with a recent analysis showing that superplastic

flow in magnesium-based alloys processed by HPT follows the conventional theoretical model for grain boundary sliding [12].

5. Summary and conclusions

1. A GW94 alloy with an initial grain size of ~8.6 μm was processed by HPT at room temperature to produce refined grain sizes of ~95 ± 10 and ~85 ± 10 nm after 8 and 16 turns, respectively. The average grain size of 85 ± 10 nm is the smallest grain size reported to date for an Mg–Gd alloy.

2. Shear punch testing was used to investigate the potential for achieving superplasticity in this alloy. A maximum strain rate sensitivity of $m \approx 0.51 \pm 0.05$ was achieved after 16 turns when testing at 623 K whereas there was grain growth and lower values of m at higher testing temperatures. The measured value for the activation energy was ~100 ± 5 kJ mol^{-1} which is consistent with grain boundary diffusion in magnesium.

3. The results suggest that the flow process in the superplastic region at 623 K is grain boundary sliding.

Acknowledgements

This work was supported in part by the European Research Council under ERC Grant Agreement No. 267464-SPDMETALS (YH and TGL).

References

[1] B.L. Mordike, T. Ebert, "Magnesium: Properties — applications — potential", Mater. Sci. Eng. A 302 (2001) 37–45.

[2] H. Watanabe, T. Mukai, M. Kohzu, S. Tanabe, K. Higashi, “Effect of temperature and grain size on the dominant diffusion process for superplastic flow in an AZ61 magnesium alloy”, Acta Mater. 47 (1999) 3753–3758.

[3] Y.H. Wei, Q.D. Wang, Y.P. Zhu, H.T. Zhou, W.J. Ding, Y. Chino, M. Mabuchi, “Superplasticity and grain boundary sliding in rolled AZ91 magnesium alloy at high strain rates”, Mater. Sci. Eng. A 360 (2003) 107–115.

[4] L. Lin, W. Wu, L. Yang, L. Chen and Z. Liu, “Grain boundary sliding and accommodation mechanisms during superplastic deformation of ZK40 alloy processed by ECAP”, J. Mater. Sci. 41 (2006) 409–415.

[5] X. Zhang, L. Li, Y. Deng, N. Zhou, “Superplasticity and microstructure in Mg–Gd–Y–Zr alloy prepared by extrusion”, J. Alloys Compd. 481 (2009) 296–300.

[6] R. Alizadeh, R. Mahmudi, T.G. Langdon, “Superplasticity of a fine-grained Mg–9Gd–4Y–0.4Zr alloy evaluated using shear punch testing”, J. Mater. Res. Technol. 3 (2014) 228–232.

[7] B.L. Xiao, Q. Yang, J. Yang, W.G. Wang, G.M. Xie, Z.Y. Ma, “Enhanced mechanical properties of Mg–Gd–Y–Zr casting via friction stir processing”, J. Alloys Compd. 509 (2011) 2879–2884.

[8] Q. Yang, B.L. Xiao, Q. Zhang, M.Y. Zheng, Z.Y. Ma, “Exceptional high-strain-rate superplasticity in Mg–Gd–Y–Zn–Zr alloy with long-period stacking ordered phase”, Scr. Mater. 69 (2013) 801–804.

[9] Q. Yang, B.L. Xiao, Z.Y. Ma, “Enhanced superplasticity in friction stir processed Mg–Gd–Y–Zr alloy”, J. Alloys Compd. 551 (2013) 61–66.

[10] A.P. Zhilyaev, T.G. Langdon, “Using high-pressure torsion for metal processing: Fundamentals and applications”, Prog. Mater. Sci. 53 (2008) 893–979.

[11] M. Kawasaki, T.G. Langdon, “Principles of superplasticity in ultrafine-grained metals”, J. Mater. Sci. 42 (2007) 1782–1796.

[12] M. Kawasaki, T.G. Langdon, “Review: achieving superplasticity in metals processed by high-pressure torsion”, J. Mater. Sci. 49 (2014) 6487–6496.

[13] Y. Harai, M. Kai, K. Kaneko, Z. Horita, T.G. Langdon, “Microstructural and mechanical characteristics of AZ61 magnesium alloy processed by high-pressure torsion”, Mater. Trans. 49 (2008) 76–83.

[14] S.A. Torbati-Sarraf, T.G. Langdon, “Mechanical properties of ZK60 magnesium alloy processed by high-pressure torsion”, Adv. Mater. Res. 922 (2014) 767–772.

[15] S.A. Torbati-Sarraf, T.G. Langdon, “Properties of a ZK60 magnesium alloy processed by high-pressure torsion”, J. Alloys Compd. 613 (2014) 357–363.

[16] M. Kai, Z. Horita, T.G. Langdon, “Developing grain refinement and superplasticity in a magnesium alloy processed by high pressure torsion”, Mater. Sci. Eng. A 488 (2008) 117–124.

[17] O.B. Kulyasova, R.K. Islamgaliev, A.R. Kil'mametov, R.Z. Valiev, "Superplastic behavior of magnesium-based Mg–10 wt%Gd alloy after severe plastic deformation by torsion", Phys. Met. Metall. 101 (2006) 585–590.

[18] A.S.J. Al-Zubaydi, A.P. Zhilyaev, S.C. Wang, P.A.S. Reed, "Superplastic behavior of AZ91 magnesium alloy processed by high-pressure torsion", Mater. Sci. Eng. A 637 (2015) 1–11.

[19] H. Matsunoshita, K. Edalati, M. Furui, Z. Horita, "Ultrafine-grained magnesium–lithium alloy processed by high-pressure torsion: Low-temperature superplasticity and potential for hydroforming", Mater. Sci. Eng. A 640 (2015) 443–448.

[20] T.G. Langdon, "Seventy-five years of superplasticity: historic developments and new opportunities", J. Mater. Sci. 44 (2009) 5998–6010.

[21] R. Mahmudi, R. Alizadeh, S. Azhari, "Strain rate sensitivity of equal-channel angularly pressed Sn–5Sb alloy determined by shear punch test", Mater. Lett. 97 (2013) 44–46.

[22] M. Karami, R. Mahmudi, "Shear punch superplasticity in equal-channel angularly pressed Mg–12Li–1Zn alloy", Mater. Sci. Eng. A 576 (2013) 156–159.

[23] N. Fakhar, F. Fereshteh-Saniee, R. Mahmudi, "High strain-rate superplasticity of fine- and ultrafine-grained AA5083 aluminum alloy at intermediate temperatures", Mater. Design 85 (2015) 342–348.

[24] M. Sarebanzadeh, R. Roumina, R. Mahmudi, G.H. Wu, H.R. Jafari Nodooshan, "Enhancement of superplasticity in a fine-grained Mg–3Gd–1Zn alloy processed by equal-channel angular pressing", Mater. Sci. Eng. A, 2015, doi: 10.1016/j.msea.2015.08.074.

[25] G.L. Hankin, M.B. Toloczko, M.L. Hamilton, R.G. Faulkner, "Validation of the shear punch-tensile correlation technique using irradiated materials", J. Nucl. Mater. 258–263 (1998) 1651–1656.

[26] R.B. Figueiredo, P.R. Cetlin, T.G. Langdon, "Using finite element modeling to examine the flow processes in quasi-constrained high-pressure torsion", Mater. Sci. Eng. A 528 (2011) 8198–8204.

[27] R. Alizadeh, R. Mahmudi, "Evaluating high-temperature mechanical behavior of cast Mg–4Zn–*x*Sb magnesium alloys by shear punch testing", Mater. Sci. Eng. A 527 (2010) 3975–3983.

[28] G.L. Hankin, M.B. Toloczko, K.I. Johnson, M.A. Khaleel, M.L. Hamilton, F.A. Garner, R.W. Davies, R.G. Faulkner, ASTM STP 1366 (2000) 1018–1028.

[29] R.Z. Valiev, Yu.V. Ivanisenko, E.F. Rauch, B. Baudelet, "Structure and deformation behaviour of Armco iron subjected to severe plastic deformation", Acta Mater. 44 (1996) 4705–4712.

[30] R. Alizadeh, R. Mahmudi, A.H.W. Ngan, T.G. Langdon, "Microstructural stability and grain growth kinetics in an extruded fine-grained Mg–Gd–Y–Zr alloy", J. Mater. Sci. 50 (2015) 4940–4951.

[31] S.S. Vagarali, T.G. Langdon, “Deformation mechanisms in h.c.p. metals at elevated temperatures—I. Creep behavior of magnesium”, Acta. Metall. 29 (1981) 1969–1982.

[32] Y. Zhenzhen, C. Hahn, “Influence of twinning on the grain refinement during high-temperature deformation in a magnesium alloy”, Scrip Mater. 64 (2011) 434–437.

[33] N.A. Smirnova, V.I. Levit, V.P. Pilyugin, R.I. Kuznetsov, M.V. Degtyarev, “Peculiarities of low-temperature recrystallization of nickel and copper”, Fiz. Metal. Metalloved 62 (1986) 566–570.

[34] C.I. Chang,X.H. Du, J.C. Huang, “Producing nanograined microstructure in Mg–Al–Zn alloy by two-step friction stir processing”, Scr. Mater. 59 (2008) 356–359.

[35] H.Q. Sun, Y.-N. Shi, M.-X. Zhang, K. Lu, “Plastic strain-induced grain refinement in the nanometer scale in a Mg alloy”, Acta Mater. 55 (2007) 975–982.

[36] S.K. Das, Y.M. Kim, T.K. Ha, R. Gauvin, I.H. Jung, “Anisotropic diffusion behavior of Al in Mg: Diffusion couple study using Mg single crystal”, Metall. Mater. Trans. A 44 (2013) 2539–2547.

[37] S.K. Das, Y.B. Kang, T. Ha, I.H. Jung, “Thermodynamic modeling and diffusion kinetic experiments of binary Mg–Gd and Mg–Y systems”, Acta Mater. 71 (2014) 164–175.

[38] Z. Yang, Z.H. Wang, H.B. Duan, Y.C. Guo, P.H. Gao, J.P. Li, "Microstructure evolution of Mg–6Gd–2Y alloy during solid solution and aging process", Mater. Sci, Eng. A 631 (2015) 160–165.

[39] S.M. He, X.Q. Zeng, L.M. Peng, X. Gao, J.F. Nie, W.J. Ding, "Microstructure and strengthening mechanism of high strength Mg–10Gd–2Y–0.5Zr alloy", J. Alloys Compd. 427 (2007) 316–323.

[40] ASM Handbook, Alloy Phase Diagrams (Vol. 3), 1992, ASM International, U.S.A.

[41] T.G. Langdon, "A unified approach to grain boundary sliding in creep and superplasticity", Acta Metall. Mater. 42 (1994) 2437–2443.

[42] H.J. Frost, M.F. Ashby, *Deformation-Mechanism Maps: The Plasticity and Creep of Metals and Ceramics*, Pergamon Press, Oxford, U.K. (1982).

Legends

Fig. 1. SEM micrographs of the alloy after (a) 1/2 , (b) 2 , (c) 8 and (d) 16 turns.

Fig. 2. TEM images of the material after (a) 8 and (b) 16 turns.

Fig. 3. TEM micrograph of the material (a) after 8 turns and corresponding elemental maps of (b) Mg, (c) Gd (c) and (d) Y.

Fig. 4. TEM micrograph of the material (a) after 16 turns and corresponding elemental maps of (b) Mg, (c) Gd and (d) Y.

Fig. 5. TEM micrograph of the material after 8 HPT turns, showing (a) a cuboidal precipitate and EDS results and (b) related SAED pattern with zone axis parallel to [103].

Fig. 6. (a) SPT curves of the material after 8 turns at 623 K, (b) normalized USS of the material after 8 turns as a function of temperature-compensated shear strain rate at different temperatures and (c) variations of *m*-value with temperature after 8 turns.

Fig. 7. TEM and SEM micrographs of the material after 8 turns following high temperature exposure at (a) 623 K and (b) 723 K.

Fig. 8. (a) Normalized USS of the material after different turns as a function of temperature-compensated shear strain rate and (b) variation of *m*-value with numbers of turns.

Fig. 9. Temperature dependence of normalized τ_m values at constant temperature-compensated shear strain rates for the alloy after 8 turns.

Table 1. Summary of superplasticity data in ultrafine- and nano-grained magnesium alloys processed by HPT [13–19].

Table 2. Summary of superplasticity data for different materials investigated by SPT [6,21–24].

Table 3. Equivalent imposed strain for different numbers of turns (at r = 1.5 mm).

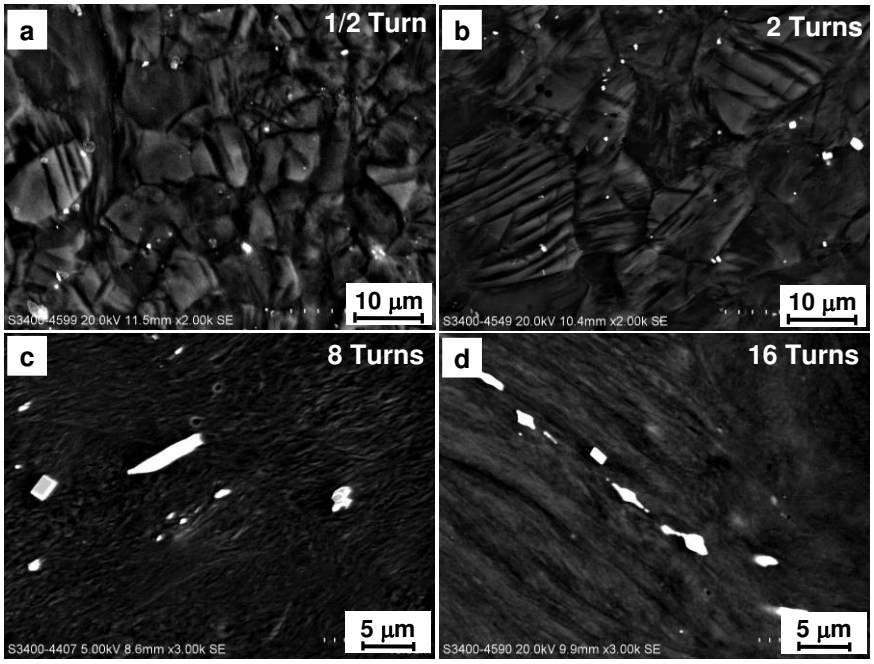

Fig. 1. SEM micrographs of the alloy after (a) 1/2 , (b) 2 , (c) 8 and (d) 16 turns.

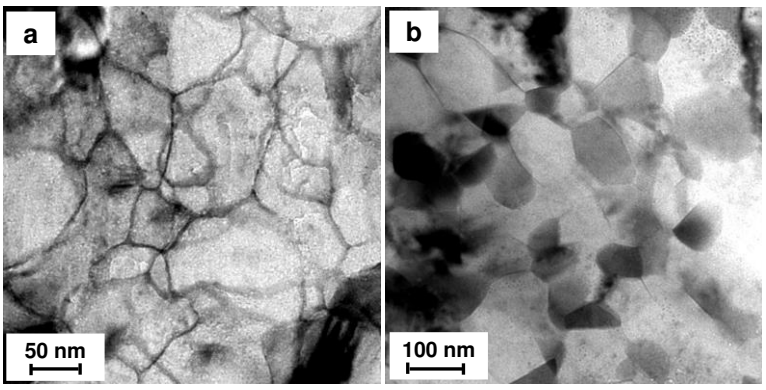

Fig. 2. TEM images of the material after (a) 8 and (b) 16 turns.

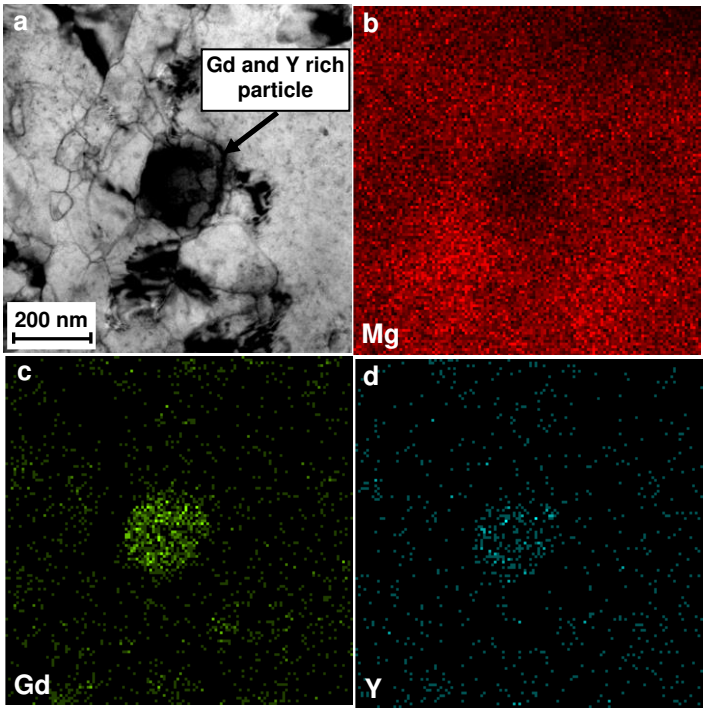

Fig. 3. TEM micrograph of the material (a) after 8 turns and corresponding elemental maps of (b) Mg, (c) Gd (c) and (d) Y.

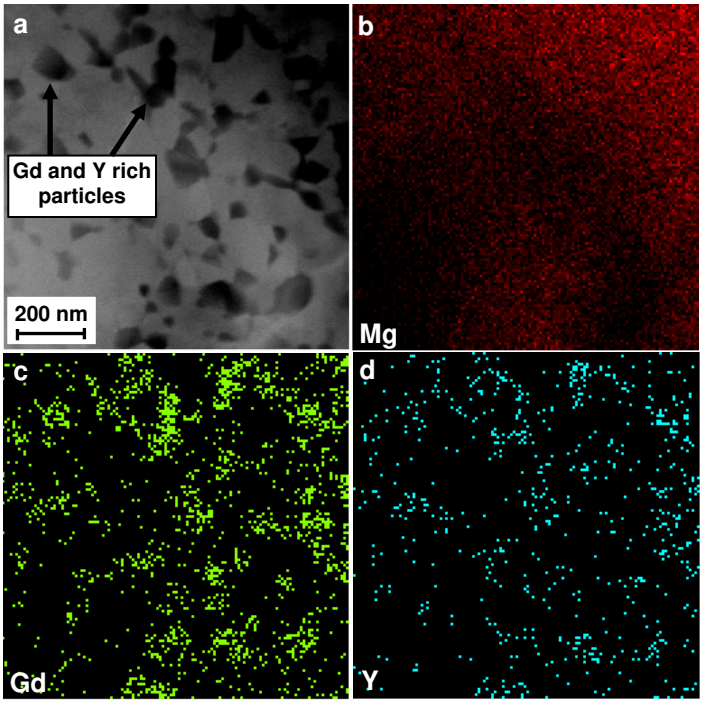

Fig. 4. TEM micrograph of the material (a) after 16 turns and corresponding elemental maps of (b) Mg, (c) Gd and (d) Y.

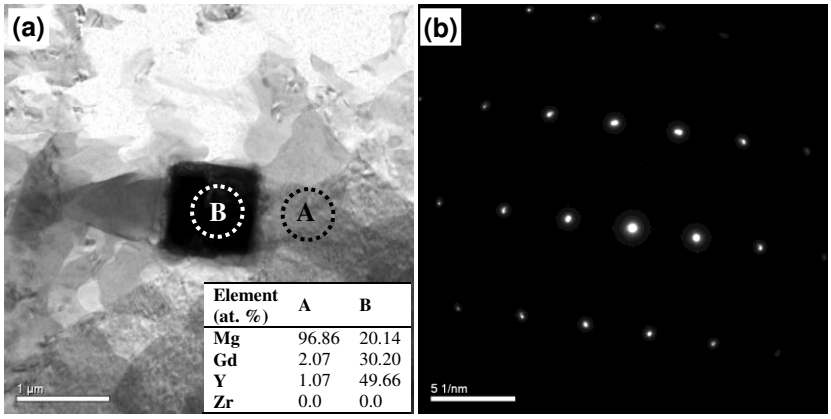

Element (at. %)	A	B
Mg	96.86	20.14
Gd	2.07	30.20
Y	1.07	49.66
Zr	0.0	0.0

Fig. 5. TEM micrograph of the material after 8 HPT turns showing (a) a cuboidal precipitate and EDS results and (b) related SAED pattern with zone axis parallel to [103].

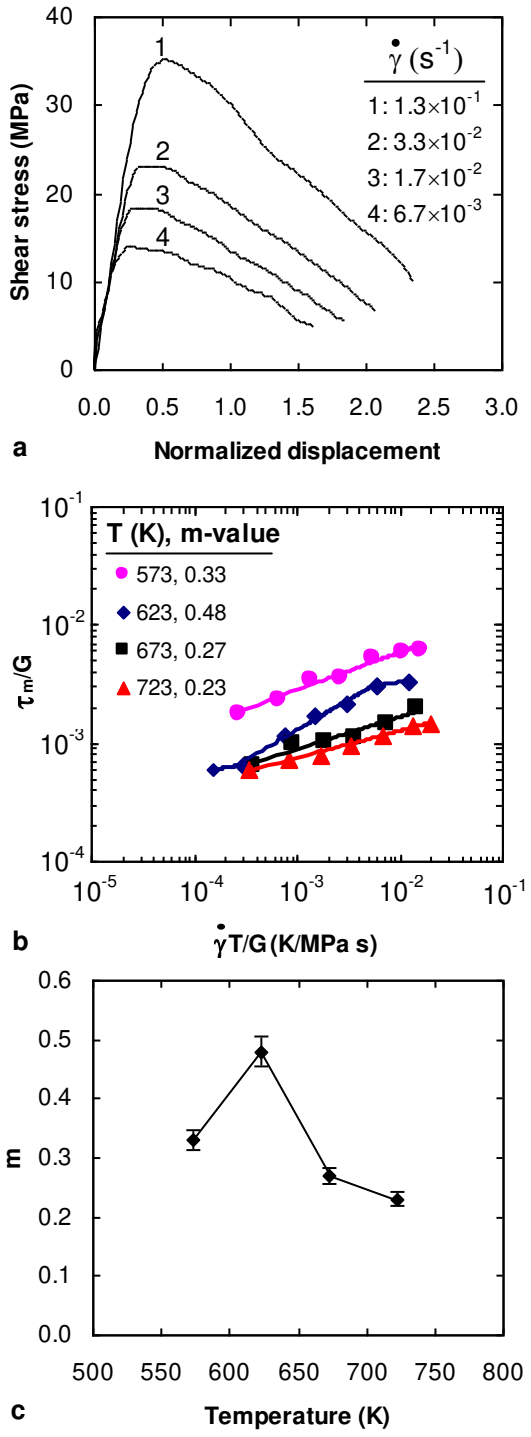

Fig. 6. (a) SPT curves of the material after 8 turns at 623 K, (b) normalized USS of the material after 8 turns as a function of temperature-compensated shear strain rate at different temperatures and (c) variations of *m*-value with temperature after 8 turns.

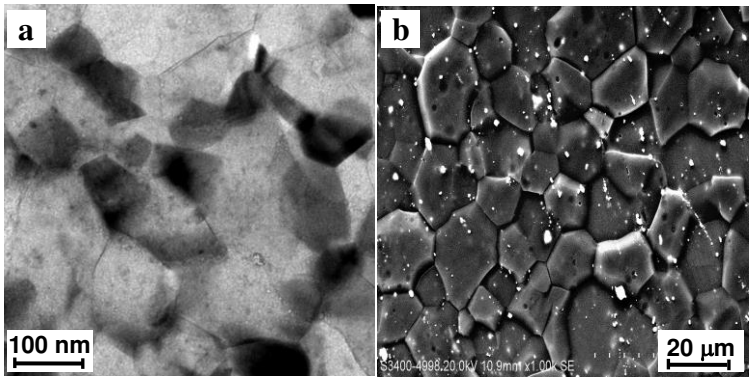

Fig. 7. TEM and SEM micrographs of the material after 8 turns following high temperature exposure at (a) 623 K and (b) 723 K.

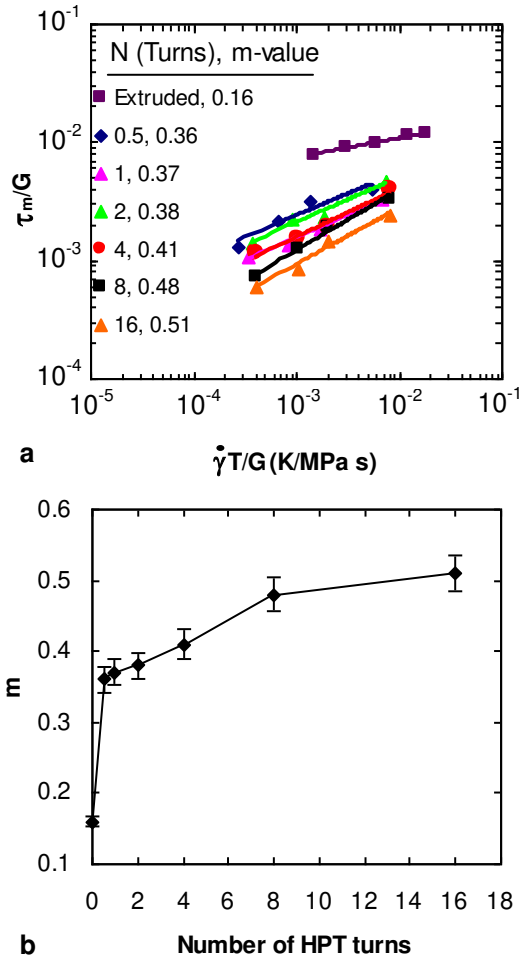

Fig. 8. (a) Normalized USS of the material after different turns as a function of temperature-compensated shear strain rate and (b) variation of *m*-value with numbers of turns.

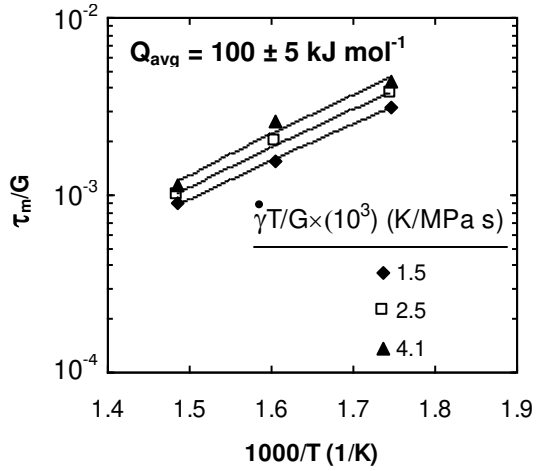

Fig. 9. Temperature dependence of normalized τ_m values at constant temperature-compensated shear strain rates for the alloy after 8 turns.

Table 1. Summary of superplasticity data in ultrafine- and nano-grained magnesium alloys processed by HPT [13-19]

Alloys or Composition (wt%)	HPT			Grain size (nm)	Superplasticity			Reference
	Number of turns	Pressure (GPa)	Temperature (K)		Testing temperature (K)	Strain rate (s^{-1})	Maximum elongation (%)	
AZ61[a]	5	3	423	230	473	3.3×10^{-3}	620	Harai *et al.* [13]
ZK60[b]	5	2	RT (296)	900-1000	473	1.0×10^{-3}	415	Torbati-Sarraf and Langdon [14]
					523		477	
					573		508	
ZK60	5	2	RT	~1000	473	1.0×10^{-4}	535	Torbati-Sarraf and Langdon [15]
Mg-9Al[c]	5	3	RT (298)	210	473	1.0×10^{-3}	600	Kai *et al.* [16]
			423	330		5.0×10^{-3}	550	
						1.0×10^{-3}	620	
						5.0×10^{-4}	810	
Mg-9Al[d]			423	370		1.0×10^{-3}	590	
Mg-10Gd	5	6	RT	~100	673	1.0×10^{-2}	470	Kulyasova *et al.* [17]
						1.0×10^{-3}	580	
AZ91[e]	10	3	RT	?	573	1.0×10^{-4}	1308	Al-Zubaydi *et al.* [18]
Mg-8Li	5	3	RT	500	473	1.0×10^{-3}	1330	Matsunoshita *et al.* [19]

[a] AZ61: Mg–6.4Al–0.74Zn–0.35Mn-0.0012Ni-0.001Cu–0.001Fe-0.015Si
[b] ZK60: Mg–5.5Zn–0.5Zr
[c] The Mg–9Al was cast prior to HPT
[d] The Mg–9Al was cast and subsequently extruded prior to HPT
[e] AZ91: Mg-9Al-1Zn

Table 2. Summary of superplasticity data for different materials investigated by SPT [6,21-24]

Alloys or Composition (wt%)	SPD process	Superplasticity		Reference
		Testing temperature (K)	SRS value	
Sn-5Sb	ECAP[a]	RT	0.57	Mahmudi *et al.* [21]
Mg-9Gd-4Y-0.4Zr	Extrusion	723	0.40	Alizadeh *et al.* [6]
Mg–12Li–1Zn	ECAP	548	0.45	Karami and Mahmudi [22]
AA5083[b]	DECLE[c]	673	0.43	Fakhar *et al.* [23]
Mg-3Gd-1Zn	ECAP	673	0.51	Sarebanzadeh *et al.* [24]

[a] Equal channel angular pressing

b AA5083: Al-4.2%Mg-0.63%Mn-0.18%Fe

[c] Double equal channel lateral extrusion

Table 3. Equivalent imposed strain for different numbers of turns (at r = 1.5 mm)

Number of turns	0.5	1	2	4	8	16
Equivalent strain	4.5	9.1	18.1	36.3	72.5	145.0